

Two-stage Stochastic Programming for Coordinated Operation of Distributed Energy Resources in Unbalanced Active Distribution Networks with Diverse Correlated Uncertainties

Ruoxuan Leng, Zhengmao Li, and Yan Xu

Abstract—This paper proposes a stochastic programming (SP) method for coordinated operation of distributed energy resources (DERs) in the unbalanced active distribution network (ADN) with diverse correlated uncertainties. First, the three-phase branch flow is modeled to characterize the unbalanced nature of the ADN, schedule DER for three phases, and derive a realistic DER allocation. Then, both active and reactive power resources are co-optimized for voltage regulation and power loss reduction. Second, the battery degradation is considered to model the aging cost for each charging or discharging event, leading to a more realistic cost estimation. Further, copula-based uncertainty modeling is applied to capture the correlations between renewable generation and power loads, and the two-stage SP method is then used to get final solutions. Finally, numerical case studies are conducted on an IEEE 34-bus three-phase ADN, verifying that the proposed method can effectively reduce the system cost and co-optimize the active and reactive power.

Index Terms—Active distribution network (ADN), two-stage stochastic programming (SP), uncertainties, voltage/var control (VVC), battery degradation.

NOMENCLATURE

A. Sets and Indices

b, i, p	Indexes for branches, buses, and phases
N_p, N_i	Numbers of phases and candidate buses
t, N_t	Index and number of dispatch period

B. Parameters

$\Gamma_R^{p,i}, L_{ESS}^{p,i}$	Rated charging life, life cycle, and rated life cycle of battery energy storage system (ESS)
$L_{ESS,R}^{p,i}$	
$\zeta_{om}^{DE}, \zeta_{om}^{WT}$	Maintenance costs of diesel generator (DE), wind turbine (WT), photovoltaic (PV), and ESS
$\zeta_{om}^{PV}, \zeta_{om}^{ESS}$	

ζ_{em}^{DE}	Emission conversion from diesel generator (DE)
$\eta_{cur}^{WT}, \eta_{cur}^{PV}$	Wind turbine (WT) and photovoltaic (PV) power curtailment costs
η_{loss}	Unit power loss cost
$\lambda_{esc}^{\min}, \lambda_{esc}^{\max}$	The minimum and maximum allowed charging power
$\lambda_{esd}^{\min}, \lambda_{esd}^{\max}$	The minimum and maximum allowed discharging power
$\tau_{es}, \varphi_{esc}, \varphi_{esd}$	Decay rate, charging efficiency, and discharging efficiency of ESS
$C_{DE}^{up}, C_{DE}^{down}$	Start-up and shut-down costs of each DE unit
$C_{ESS,deg}^{p,i}$	Degradation cost of battery ESS
$DoD_R^{p,i}$	Rated depth of discharge (DoD)
$E_{ESS}^{\min}, E_{ESS}^{\max}$	The minimum and maximum energy stored in each ESS unit
$E_{ESS,R}^{p,i}$	Rated battery ESS capacity
$Inv_{ESS}^{p,i}$	Unit investment cost of ESS
$\ell_{pur}^t, \ell_{sell}^t$	Electricity purchasing and selling prices
$L_{ESS}^{p,i}$	Number of battery ESS life cycle
$P_{DE}^{\min}, P_{DE}^{\max}$	The minimum and maximum power output rates of DE
$P_{LD}^{p,i}, Q_{LD}^{p,i}$	Active and reactive power demands
$P_{WT,REAL}^{p,i}, P_{PV,REAL}^{p,i}$	Available energy resources from WT and PV
P_{unb}^{\max}	Hourly maximum three-phase active power unbalance limit
$Q_{CB,\min}^{p,i}, Q_{CB,\max}^{p,i}$	The minimum and maximum allowed reactive power of capacitor bank (CB)
$Q_{PV,\min}^{p,i}, Q_{PV,\max}^{p,i}$	The minimum and maximum allowed reactive power of PV
$Q_{WT,\min}^{p,i}, Q_{WT,\max}^{p,i}$	The minimum and maximum allowed reactive power of WT
$R_{DE}^{up}, R_{DE}^{down}$	Ramping-up and ramping down rates of DE

Manuscript received: August 11, 2022; revised: October 31, 2022; accepted: December 5, 2022. Date of CrossCheck: December 5, 2022. Date of online publication: January 10, 2023.

This article is distributed under the terms of the Creative Commons Attribution 4.0 International License (<http://creativecommons.org/licenses/by/4.0/>).

R. Leng, Z. Li, and Y. Xu (corresponding author) are with School of Electrical and Electronic Engineering, Nanyang Technological University, Singapore (e-mail: ruoxuan002@e.ntu.edu.sg; lizh0049@e.ntu.edu.sg; eeyanxu@gmail.com).
DOI: 10.35833/MPCE.2022.000510



S_{sub}^{\max}	The maximum transformer power limit
$U_{CB}^{p,i}, U_{tap}$	Unit adjustment levels of CB and on-load tap changer (OLTC)
Unb_{total}^{\max}	Total active three-phase power unbalance limit at the root branch
V_{\min}^2, V_{\max}^2	The minimum and maximum voltage square limits
V_{sub}	Voltage of substation
x_0, x_1	Parameters of life cycle curve fitting

C. Variables

$A_{de}^{p,i,t}$	Binary variable for DE on and off statuses
C_{curt}^t, C_{loss}^t	RES curtailment and power loss costs
C_{em}^t, C_{deg}^t	Gas emission and battery aging costs
C_{ex}^t, C_{om}^t	Power transaction and maintenance costs
C_{st}^t, C_{sd}^t	Start-up and shut-down costs
$DoD_{ESS}^{p,t,i}$	DoD of ESS units
$E_{ESS}^{p,t,i}$	Energy stored in battery ESS units
I_{ij}	Three-phase line current vector, $I_{ij} = [I_{ij}^a, I_{ij}^b, I_{ij}^c]^T \in \mathbb{C}^{3 \times 1}$
L_{ESS}^{DoD}	Functional relationship of ESS life cycle in terms of DoD
$P_{DE}^{p,t,i}, P_{WT}^{p,t,i}, P_{PV}^{p,t,i}$	DE, WT, and PV power outputs
$P_{ESC}^{p,t,i}, P_{ESD}^{p,t,i}$	Charging and discharging power of ESS
$P_{fw,a}^{p,t,0,b+1}, Q_{fw}^{p,t,0,b+1}$	Active and reactive power flowing on the lateral branch of branch $b+1$
$P_{fw,a}^{t,1}, P_{fw,b}^{t,1}, P_{fw,c}^{t,1}$	Root branch power flow for phase a, b , and c
$P_{PUR}^{p,t,i}, P_{SELL}^{p,t,i}$	Purchasing and selling power between distributed system and power grid
P_{unb}^t	Hourly root branch three-phase active power unbalance
$Q_{CB}^{p,t,i}$	Reactive power output from CB
$Q_{WT}^{p,i,t}, Q_{PV}^{p,i,t}$	WT and PV reactive power outputs
$Tap^t, I_{CB}^{p,t}$	Position levels of OLTC and CB
Tap_{\min}, Tap_{\max}	The minimum and maximum tap change ratios
U_i, U_j	Voltage vectors, $U_i = [V_i^a ^2, V_i^b ^2, V_i^c ^2]^T$ and $U_j = [V_j^a ^2, V_j^b ^2, V_j^c ^2]^T$
$U_a^{t,i}, U_b^{t,i}, U_c^{t,i}$	Bus voltage squares for phases a, b , and c
Unb^{avg}	Hourly three-phase power unbalance rate
V_i, V_j	Three-phase voltage vectors at buses i and j , $V_i = [V_i^a, V_i^b, V_i^c]^T \in \mathbb{C}^{3 \times 1}$ and $V_j = [V_j^a, V_j^b, V_j^c]^T \in \mathbb{C}^{3 \times 1}$
$\bar{Z}_{i \rightarrow j}$	Line impedance from buses i to j

z_{ij}	Line impedance matrix, denoted by the complex form of line resistance r_{ij} and reactance x_{ij} , $z_{ij} \in \mathbb{C}^{3 \times 3}$
----------	--

I. INTRODUCTION

CURRENTLY, the optimal operation of active distribution networks (ADNs) plays an essential role in the effective integration of renewable-based generators, optimal energy management, power loss reduction as well as cost saving [1]. However, with the increasing penetration of renewable energy sources (RESs) and the utilization of energy storage systems (ESSs) in real life, it is increasingly important to derive a practical ADN operation, close to the real industrial application. In this regard, developing an effective approach to support and improve ADN operation has turned into a critical concern in both academia and industry.

In practice, ADNs are generally unbalanced. For instance, the unbalanced line configuration including two- or single-phase laterals downstream of feeder backbones is common in ADN. meanwhile, the unbalanced demand consisting of single or two phases loads is prevalent [2]. Further, the excessive installation of renewable-based distributed generators (DGs) could also exacerbate power imbalance [3]. However, the existing ADN operation methods usually assume a balanced ADN where the power balance will be satisfied by equally allocated DG on each phase [4]. This assumption gives the ideal solution for DG scheduling, but it is impractical and insufficient for real-world unbalanced ADNs.

To characterize the unbalanced ADN, it is necessary to implement the three-phase power flow on the scheduling framework. In [5], a non-linear branch flow model for both mesh and radial networks is demonstrated by convexification and relaxation techniques. Reference [6] obtains the unbalanced three-phase power flow solutions via an iterative load flow method. The three-phase power flow model in both [5] and [6] would lead to a high computational burden and complicate the application process. In this case, the linearized three-phase power flow model with several assumptions developed in [7] could be utilized and the effectiveness of this method has also been validated by [3].

In addition, based on the three-phase unbalanced system structure, active and reactive power flows for the three-phase system are supposed to be co-optimized. However, traditionally, the active and reactive power for ADN operation is optimized separately [8] or the focus is on the active power scheduling only [9]. Nevertheless, the reactive power dispatch cannot be neglected as the renewable-based DGs critically affect bus voltage due to the high resistance-to-reactance ratio of distribution lines [10]. In this sense, to deal with the reactive power dispatch and regulate the voltage, the centralized voltage/var control (VVC) method can be employed. The centralized VVC permits the coordination of the heterogeneous VVC devices on account of the system-wide information to meet voltage constraints [11]. Reference [12] mitigates the voltage rise problem brought by excessive solar photovoltaic (PV) integration by a multi-objective VVC method in the ADN considering the tap movements of the

transformers and active power curtailment of RES. In [13], the VVC scheme on multiple timescales is applied for ESS dispatch in the ADN. It aims to coordinate multiple power electronic assets. Similarly, [14] presents a multi-objective VVC for ADN with RES uncertainties. The solution is obtained through a three-step method, including global/local search and user preference.

Apart from the comprehensive active and reactive power modeling, the key components in the ADN should also be characterized precisely. The ESS is a critical component in the ADN for both peak shaving and cost saving [11]. To model ESS comprehensively, the degradation process should be considered since the aging impact will be induced from each charging or discharging event [15]. Besides, the ignorance of ESS aging might lead to an underestimated system operation cost. Thus, the ESS degradation cost should be modeled for a more comprehensive and accurate ADN operation. The study in [16] formulates the nonlinear ESS degradation cost based on the depth of discharge (DoD) and lifetime. In [17], the influence of the ambient temperature is also modeled in the ESS degradation cost model. References [16] and [17] show that ESS aging has a significant impact on the system operation cost.

Finally, the uncertainties brought by RES and power load should be tackled in ADN operation. Broadly speaking, robust optimization (RO) and stochastic programming (SP) are the two main methods to address diverse uncertainties. The RO benefits from high computing efficiency, but the robust decisions hedging against the worst cases may suffer from over-conservativeness [18]. The SP, in contrast, covers a wide range of scenarios and optimizes the decisions by evaluating the expected operation cost of numerous samples [11]. Reference [19] studies the scheduling problems in ADN via the SP method considering the realistic load model and voltage security. The stochastic unit commitment in [20] coordinates both day-ahead and real-time decisions and considers the continuity among numerous periods when generating uncertain scenarios. However, the SP methods used in [19] and [20] generate scenarios and address the uncertainties separately with only independent distributions. Different from the large-scale utility network, ADN operation is usually conducted in the same region, where the accumulation of the loads has general features and strenuous correlations with RES output [21]. To capture the correlations of multiple-site RES generations and power load precisely, the copula theory has been verified to be effective in ADN operation, planning, and voltage stability problems [22]. Reference [21] employs the Gumbel copula family to deliberate the stochastic interdependence of wind turbine (WT) generation and load uncertainties for SP-based operation, in which the correlation structure in the same region is recognized by historical data. Reference [22] tackles the uncertainties of WT and load on each candidate bus by applying copula theory. To further reveal the interdependence accurately, they utilize the multivariate D-vine copula to alter the copula family case-by-case, suiting each scenario. It can be observed from [21] and [22] that considering the correlations among all uncertainty sources is necessary for deriving accurate solutions.

Given the insights above, this paper studies a two-stage SP method for the coordinated operation of the DER in unbalanced ADN considering diverse correlated uncertainties. The main research contributions are summarized as follows.

1) A comprehensive operation model for unbalanced ADN, involving the linearized three-phase branch flow model, is proposed to schedule the DG generation separately among three phases and calculate the system cost more practically and precisely.

2) The unbalanced ADN operation method can optimally dispatch the active and reactive power simultaneously by applying the VVC scheme and regulating the voltage to derive a more realistic operation. In addition, the ESS degradation model is also included to model the aging cost through each charging/discharging event to obtain more accurate solutions.

3) Diverse uncertainties from the RES generation and power loads are addressed via the copula theory to capture the correlation relationship between the output from PVs, WTs, and the demand of each phase. Then all the uncertainties are tackled via the two-stage SP method.

The rest of this paper is organized as follows. The proposed unbalanced ADN model is presented in Section II. The mathematical formulation and solution methodology are discussed in Section III and Section IV, respectively. Numerical case studies are demonstrated in Section V, and finally, the conclusion is drawn in Section VI.

II. UNBALANCED ADN MODEL

A. Framework of Unbalanced ADN

The framework of unbalanced ADN is provided in Fig. 1, involving both active and reactive power flows. The active power load can be supplied by diesel generator (DE), WT, PV, and the power transaction with the main grid. The reactive power can be supported by capacitor bank (CB), on-load tap changer (OLTC), and electronic converter of renewable-based DG. For the ESS, we focus only on battery storage in this paper, which enables load shifting and dispatch flexibility enhancement through each charging or discharging event [11].

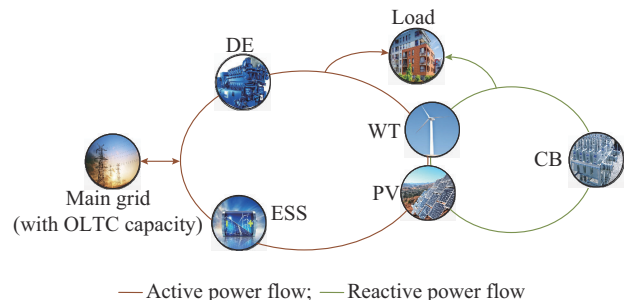


Fig. 1. Framework of unbalanced ADN.

B. Linear Three-phase Power Flow Model

In general, the ADN is unbalanced. The relatively high degree of unbalance is caused by the naturally transposed architecture of three-phase distribution lines, the existence of single-phase laterals, single- and double-phase loads, or unbal-

anced three-phase loads [2]. The increasing installation of single-phase or double-phase renewable DG also induces several impacts on ADN such as voltage rise, reverse power flow, and voltage imbalance. However, most of the research outcomes of ADN operation in [16]-[21] assume that a single-phase system for simplicity is not as accurate as the effects of system imbalance are regarded as negligible. This could result in underestimating system operation cost and an idealistic scheduling result. Based on the insight above, it is necessary to develop a three-phase system for the study of unbalanced ADN operation.

In this paper, the linearized three-phase branch flow model developed in [7] is incorporated into the proposed model as part of the network operation constraints. The effectiveness of this model has been validated by the application of ADN hosting capacity improvement [3], distribution system restoration [23], and VVC [24] problems. The detailed three-phase power flow model is illustrated as follows.

In this model, we first apply Kirchhoff's voltage law for each line connected to an ordered buses pair $(i,j) \in \mathfrak{I}$ and the voltage relationship can be obtained as:

$$V_j = V_i - z_{ij} I_{ij} \quad (1)$$

I_{ij} is expressed in (2), and * denotes conjugate.

$$I_{ij} = \mathbf{S}_{ij}^* \oslash \mathbf{V}_i^* \quad (2)$$

Substituting (2) into (1) and multiplying both sides by their complex conjugate, we can obtain (3), where $\mathbf{S}_{ij} = [P_{ij}^a + jQ_{ij}^a, P_{ij}^b + jQ_{ij}^b, P_{ij}^c + jQ_{ij}^c]^T \in \mathbb{C}^{3 \times 1}$ is the apparent branch power of bus pair $(i,j) \in \mathfrak{I}$. Operators \oslash and \odot in the model denote the elementwise division and multiplication, respectively.

$$V_j \odot V_j^* = V_i \odot V_i^* - z_{ij} (\mathbf{S}_{ij}^* \oslash \mathbf{V}_i^*) \odot V_i^* - z_{ij}^* (\mathbf{S}_{ij} \oslash \mathbf{V}_i) \odot V_i + \mathbf{c}_{ij}(\mathbf{S}_{ij}, V_i, z_{ij}) \quad (3)$$

where the last term $\mathbf{c}_{ij}(\mathbf{S}_{ij}, V_i, z_{ij})$ is the higher-order term. To conduct the linear approximation of power flow, the following two assumptions are made in [7] and applied.

1) Line power losses are small, i. e., $\mathbf{c}_{ij}(\mathbf{S}_{ij}, V_i, z_{ij}) \ll \mathbf{S}_{ij}$, which can be neglected in the model.

2) Voltages are nearly balanced, so we have:

$$V_i^a/V_i^b \approx V_i^b/V_i^c \approx V_i^c/V_i^a \approx e^{j2\pi/3} \quad (4)$$

Therefore, substituting (4) into (3) and omitting the higher-order term \mathbf{c}_{ij} , (3) can be simplified as:

$$U_j = U_i - \bar{z}_{ij} \mathbf{S}_{ij}^* - \bar{z}_{ij}^* \mathbf{S}_{ij} \quad (5)$$

The impedance matrix $\bar{z}_{ij} = \partial \odot z_{ij} \in \mathbb{C}^{3 \times 3}$, and ∂ is denoted as:

$$\partial = \begin{bmatrix} 1 & e^{-j2\pi/3} & e^{j2\pi/3} \\ e^{j2\pi/3} & 1 & e^{-j2\pi/3} \\ e^{-j2\pi/3} & e^{j2\pi/3} & 1 \end{bmatrix} \quad (6)$$

Combined with the power balance constraints for the proposed unbalanced ADN operation model, the linearized three-phase power flow can be formulated in (7)-(9).

$$P_{flw}^{p,t,b+1} = P_{flw}^{p,t,b} - P_{flw}^{p,t,0,b+1} - P_{LD}^{p,t,i} + P_{DE}^{p,t,i} + P_{PV}^{p,t,i} + P_{WT}^{p,t,i} + P_{ESD}^{p,t,i} - P_{ESC}^{p,t,i} + P_{PUR}^{p,t,i} - P_{SELL}^{p,t,i} \quad (7)$$

$$Q_{flw}^{p,t,b+1} = Q_{flw}^{p,t,b} - Q_{flw}^{p,t,0,b+1} - Q_{LD}^{p,t,i} + Q_{PV}^{p,t,i} + Q_{WT}^{p,t,i} + Q_{CB}^{p,t,i} \quad (8)$$

$$\begin{bmatrix} U_a^{t,i+1} \\ U_b^{t,i+1} \\ U_c^{t,i+1} \end{bmatrix} = \begin{bmatrix} U_a^{t,b} \\ U_b^{t,b} \\ U_c^{t,b} \end{bmatrix} - \bar{Z}_{i \rightarrow j} \begin{bmatrix} P_{flw,a}^{t,b} - jQ_{flw,a}^{t,b} \\ P_{flw,b}^{t,b} - jQ_{flw,b}^{t,b} \\ P_{flw,c}^{t,b} - jQ_{flw,c}^{t,b} \end{bmatrix} - \bar{Z}_{i \rightarrow j}^* \begin{bmatrix} P_{flw,a}^{t,b} + jQ_{flw,a}^{t,b} \\ P_{flw,b}^{t,b} + jQ_{flw,b}^{t,b} \\ P_{flw,c}^{t,b} + jQ_{flw,c}^{t,b} \end{bmatrix} \quad (9)$$

Equations (7) and (8) denote the active and reactive power flows of the distribution network, respectively. Equation (9) calculates the square of the three-phase bus voltage magnitude.

C. ESS Degradation Modeling

The life cycle of ESS units can be used to evaluate the ESS degradation through each charging or discharging process [11]. For ESS operation, the influential factors include cycle depth, charging/discharging power, and state of charge. The life cycle of each ESS unit, or the number of charging/discharging cycles within its useful life, can be denoted by effective cumulative ampere-hours throughput at the rated discharged rate and rated DoD before its capacity drops below 80% of its rated capacity [15]. As an essential factor, DoD indicates the discharging percentage of the battery relative to its total capacity, as shown in (10). The rated charging life of ESS is represented in (11).

$$DoD^{p,i,t} = 1 - E_{ESS}^{p,i,t} / E_{ESS,R}^{p,i} \quad (10)$$

$$\Gamma_R^{p,i,t} = L_{ESS}^{p,i,t} \cdot DoD^{p,i,t} \cdot E_{ESS,R}^{p,i} \quad (11)$$

The relationship between expected average cycle and DoD for the Li-ion battery is shown in Fig. 2, which can be obtained via the curve fitting method, based on the data provided by a different manufacturer. The detailed curve fitting method can be referred to [25] and the mathematical expression for the ESS life cycle is represented in (12), which can be applied to other batteries with different fitting parameters [15].

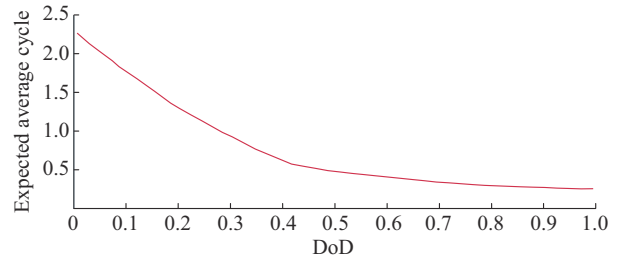


Fig. 2. Relationship between expected average cycle and DoD.

Based on the definitions above, the ESS degradation cost model for each charging/discharging event can be identified in (13).

$$L_{ESS}^{DoD} = L_{ESS,R}^{p,i} \left(\frac{DoD^{p,i}}{DoD_{ESS}^{p,i}} \right)^{X_0} e^{X_1} \left(1 - \frac{DoD_{ESS}^{p,i}}{DoD^{p,i}} \right) \quad (12)$$

$$C_{ESS,deg}^{p,i,t} = Inv_{ESS}^{p,i} \cdot L_{ESS,R}^{p,i} / L_{ESS}^{p,i,t} \cdot DoD^{p,i,t} \cdot E_{ESS,R}^{p,i} \quad (13)$$

III. PROBLEM FORMULATION

The mathematical formulation of the proposed method is described based on a typical unbalanced ADN. The active power scheduling of DE, WT, PV, and ESS can be optimized, for the reactive power dispatch, operation schedules

of the CB, OLTC, and the electronic converters for WT and PV would be decided. The overall deterministic ADN operation model is given as follows.

1) Objective function: the proposed unbalanced ADN operation aims at minimizing the system operation cost as:

$$C_{system} = \min \sum_{t \in N_t} C_{Total}^t \Delta t \quad (14)$$

$$C_{Total}^t = C_{ex}^t + C_{om}^t + C_{em}^t + C_{deg}^t + C_{curt}^t + C_{loss}^t + C_{st}^t + C_{sd}^t \quad (15)$$

$$C_{ex}^t = \sum_{p \in N_p} \sum_{i \in N_i} (\ell_{pur}^t P_{PUR}^{p,t,i} - \ell_{sell}^t P_{SELL}^{p,t,i}) \quad (16)$$

$$C_{om}^t = \sum_{p \in N_p} \sum_{i \in N_i} [\zeta_{om}^{DE} P_{DE}^{p,t,i} + \zeta_{om}^{WT} P_{WT}^{p,t,i} + \zeta_{om}^{PV} P_{PV}^{p,t,i} + \zeta_{om}^{ESS} (P_{ESC}^{p,t,i} + P_{ESD}^{p,t,i})] \quad (17)$$

$$C_{em}^t = \sum_{p \in N_p} \sum_{i \in N_i} \zeta_{em}^{DE} P_{DE}^{p,t,i} \quad (18)$$

$$C_{deg}^t = \sum_{p \in N_p} \sum_{i \in N_i} C_{ESS_{deg}}^{p,t,i} (P_{ESC}^{p,t,i} + P_{ESD}^{p,t,i}) \quad (19)$$

$$C_{curt}^t = \sum_{p \in N_p} \sum_{i \in N_i} [\eta_{cur}^{WT} (P_{WT,real}^{p,t,i} - P_{WT}^{p,t,i}) + \eta_{cur}^{PV} (P_{PV,real}^{p,t,i} - P_{PV}^{p,t,i})] \quad (20)$$

$$C_{loss}^t = \sum_{p \in N_p} \sum_{b \in N_b} \eta_{loss} R_b [(P_{flw}^{p,t,b})^2 + (Q_{flw}^{p,t,b})^2] / V_{sub}^2 \quad (21)$$

$$C_{st}^t = \sum_{p \in N_p} \sum_{i \in N_i} \max \{0, A_{de}^{p,t,i} - A_{de}^{p,t-1,i}\} C_{DE}^{up} \quad (22)$$

$$C_{sd}^t = \sum_{p \in N_p} \sum_{i \in N_i} \max \{0, A_{de}^{p,t-1,i} - A_{de}^{p,t,i}\} C_{DE}^{down} \quad (23)$$

Equation (14) is the objective function of the proposed model indicating the minimization of system operation cost. Equation (15) denotes the operation cost including power exchange cost with the main grid (16), maintenance cost of each DER unit (17), gas emission cost of DE (18), ESS degradation cost (19), RES curtailment cost (20), power loss cost (21), start-up cost (22), and shut-down cost of DE (23).

2) Constraints:

$$A_{de}^{p,t,i} P_{DE}^{\min} \leq P_{DE}^{p,t,i} \leq A_{de}^{p,t,i} P_{DE}^{\max} \quad (24)$$

$$R_{DE}^{down} \Delta t \leq P_{DE}^{p,t,i} - P_{DE}^{p,t-1,i} \leq R_{DE}^{up} \Delta t \quad (25)$$

$$[P_{WT}^{p,t,i}, P_{PV}^{p,t,i}] \leq [P_{WT,REAL}^{p,t,i}, P_{PV,REAL}^{p,t,i}] \quad (26)$$

$$\begin{cases} [Q_{WT}^{p,t,i}, Q_{PV}^{p,t,i}] \geq [Q_{WT,\min}^{p,i}, Q_{PV,\min}^{p,i}] \\ [Q_{WT}^{p,t,i}, Q_{PV}^{p,t,i}] \leq [Q_{WT,\max}^{p,i}, Q_{PV,\max}^{p,i}] \end{cases} \quad (27)$$

$$\begin{cases} [P_{ESC}^{p,t,i}, P_{ESD}^{p,t,i}] \geq [\lambda_{esc}^{\min}, \lambda_{esd}^{\min}] E_{ESS}^{p,i} \\ [P_{ESC}^{p,t,i}, P_{ESD}^{p,t,i}] \leq [\lambda_{esc}^{\max}, \lambda_{esd}^{\max}] E_{ESS}^{p,i} \end{cases} \quad (28)$$

$$P_{ESC}^{p,t,i} P_{ESD}^{p,t,i} = 0 \quad (29)$$

$$E_{ESS}^{\min} \leq E_{ESS}^{p,t,i} \leq E_{ESS}^{\max} \quad (30)$$

$$E_{ESS}^{p,t,i} = (1 - \tau_{es}) E_{ESS}^{p,t-1,i} + (P_{ESC}^{p,t,i} \varphi_{esc} - P_{ESD}^{p,t,i} / \varphi_{esd}) \Delta t \quad (31)$$

$$E_{ESS}^{p,0,i} = E_{ESS}^{p,N_t \Delta t,i} \quad (32)$$

$$\begin{cases} |P_{flw,a}^{t,1} - P_{flw,b}^{t,1}| \leq P_{flw}^t \leq P_{flw}^{\max} \\ |P_{flw,b}^{t,1} - P_{flw,c}^{t,1}| \leq P_{flw}^t \leq P_{flw}^{\max} \\ |P_{flw,c}^{t,1} - P_{flw,a}^{t,1}| \leq P_{flw}^t \leq P_{flw}^{\max} \end{cases} \quad (33)$$

$$\sum_{t \in N_t} P_{unb}^t \leq Unb_{total}^{\max} \quad (34)$$

$$(P_{flw}^{p,t,1})^2 + (Q_{flw}^{p,t,1})^2 \leq (S_{sub}^{\max})^2 \quad (35)$$

$$V_{bus}^{t,0} = V_{sub} + Tap^t \cdot U_{tap} \quad (36)$$

$$Tap_{\min} \leq Tap^t \leq Tap_{\max} \quad (37)$$

$$Q_{CB}^{p,t,i} = I_{CB}^{p,t} U_{CB}^{p,i} \quad (38)$$

$$Q_{CB,\min}^{p,i} \leq Q_{CB}^{p,t,i} \leq Q_{CB,\max}^{p,i} \quad (39)$$

$$V_{\min}^2 \leq [U_a^{t,i}, U_b^{t,i}, U_c^{t,i}] \leq V_{\max}^2 \quad (40)$$

Formulas (24) and (25) are the operation constraints for DEs to ensure the power boundary and ramping rate within the allowed range; (26) denotes that the RES generation cannot exceed the available resources; (27) shows the reactive power limits of RES units; (28)-(32) are the operation constraints for ESS; (28) and (29) denote that the charging and discharging power should be within the capacity boundary; meanwhile, the charging and discharging events of the ESS cannot happen at the same time; (30) denotes the ESS energy capacity limits and (31) builds the relationship of the energy stored in ESS and its charging/discharging power; (32) ensures the same ESS scheduling flexibility of each dispatch period where the starting energy should be equal to the ending energy [11]; (33) and (34) are the constraints of three-phase power unbalance, indicating the root branch unbalance at each time interval and the overall power unbalance should be within the pre-defined limits; (35) denotes that the root branch apparent power should be within the power limit of substation; (36) - (39) are the constraints related to VVC scheme [10]; (36) denotes that the voltage of the reference bus is defined based on the tap position of OLTC; (37) indicates the tap position limits of OLTC; (38) indicates the reactive output from CB units, which is discreetly relying on its tap position; (39) shows the reactive output limits of CB units; and (40) limits the bus voltage of each phase within the safety range [3].

IV. SOLUTION METHODOLOGY

A. Model Linearization and Relaxation

The mathematical function of the proposed model in (14)-(40) is nonlinear due to the nonlinear constraints (12), (13), and (21)-(23). Solving the nonlinear term directly is time-consuming and ineffective. To release the computation burden and improve the solution accuracy, the linearization and relaxation methods are adopted in this paper.

1) Piecewise Linearization

Equations (19) and (21) are nonlinear functions that can be linearized by introducing a number of sampling coordinates on the x -axis within an independent variable domain. To make it clear, taking the nonlinear function in Fig. 3 for illustration, it can be approximated by the summation of linear segments $[(x_i, f(x_i)), (x_{i+1}, f(x_{i+1}))]$ in which $i \in [1, n-1]$, x is the decision variable, and $f(x)$ is the objective function.

$$f_{obj} = \sum_{i=1}^n (k_i x + \mu_i b_i) \quad (41)$$

$$k_i = (f(x_{i+1}) - f(x_i)) / (x_{i+1} - x_i) \quad (42)$$

$$\begin{cases} \mu_i x_i \leq x \leq \mu_{i+1} x_{i+1} \\ \sum_{i=1}^n \mu_i \leq 1 \end{cases} \quad (43)$$

In (41), each linear segment can be expressed by the slope k_i and intercept b_i . The binary variable μ_i denotes the binary state of each linear block, as shown in (43).

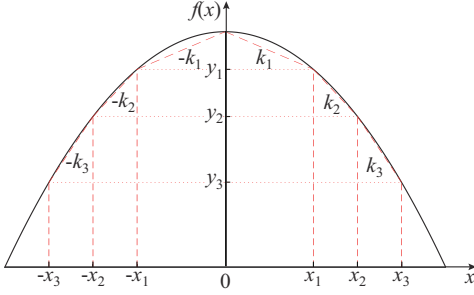


Fig. 3. Piecewise linear relaxation of a convex quadratic function.

2) Max Function Relaxation

The start-up cost (22) and shut-down cost (23) functions are max functions. The linear relaxation of the max function is obtained by splitting the max function into two individual expressions, seeking for their supremum as:

$$\begin{cases} C_{st}^t \geq \sum_{p \in N_p} \sum_{i \in N_i} (A_{de}^{p,t,i} - A_{de}^{p,t-1,i}) C_{DE}^{up} & C_{st}^t \geq 0 \\ C_{sd}^t \geq \sum_{p \in N_p} \sum_{i \in N_i} (A_{de}^{p,t-1,i} - A_{de}^{p,t,i}) C_{DE}^{down} & C_{sd}^t \geq 0 \end{cases} \quad (44)$$

B. Copula-based Uncertainty Description Method

To describe the stochastic interdependence between uncertain variables (WT, PV, and power load), the copula function is demonstrated here to capture the correlations between them. The stochastic scenarios are then involved in the unbalanced ADN operation model to address uncertainties.

The copula is a multivariate cumulative distribution with uniform marginals of each variable on the interval $[0, 1]$ [26]. According to Sklar's theorem [27], [28], the foundation of copula theory defines that any K -dimensional random input variables $\{x_1, x_2, \dots, x_K\}$ with marginals $\{F_1(x_1), F_2(x_2), \dots, F_K(x_K)\}$ link by a copula c to express their joint cumulative distribution function F_K , as shown in (45).

$$F_K(x) = C(F_1(x_1), F_2(x_2), \dots, F_K(x_K)) \quad (45)$$

Hence, differentiating (45), the joint probability distribution function of variables x_1, x_2, \dots, x_K can be obtained, as shown in (46), in which the copula density function is formulated as (47). The conditional density functions can be expressed as (48).

$$f(x) = C(F_1(x_1), F_2(x_2), \dots, F_K(x_K)) \sum_{k=1}^K f_k(x_k) \quad (46)$$

$$C(x) = C(x_1, x_2, \dots, x_K) = \frac{\partial^K C(x_1, x_2, \dots, x_K)}{\partial x_1 \partial x_2 \dots \partial x_K} \quad (47)$$

$$f(x_1 | x_1, x_2, \dots, x_K) = f(x) / \sum_{k=1}^K f_k(x_k) = c(F_1(x_1), F_2(x_2), \dots, F_K(x_K)) f_1(x_1) \quad (48)$$

For the high-dimensional models, various pair copulas will be constructed for scenario generation to reveal the hidden association of uncertain variables. In this paper, the Gaussian and Gumbel copula families are utilized whose cumulative distribution functions are expressed as (49) and (50). φ is the univariate standard normal distribution; $\varphi_{2,\theta}$ is the bivariate normal distribution with zero means; θ is the unit variance and correlation parameter [26]; and \inf is the general term to show infinity.

$$C_{Gau} = \varphi_{2,\theta}(\varphi^{-1}(\alpha), \varphi^{-1}(\beta))^{(\nu)} \quad \theta \in (-1, 1) \quad (49)$$

$$C_{Gum} = \exp(-((-\lg \alpha)^\theta + (-\lg \beta)^\theta)^{\frac{1}{\theta}}) \quad \theta \in [1, \inf) \quad (50)$$

C. Two-stage Coordinated Structure

To handle the various uncertainties, the proposed operation model is converted to a two-stage SP problem indicated in Fig. 4, which includes both day-ahead (first-stage) and intra-day (second-stage) timeframes.

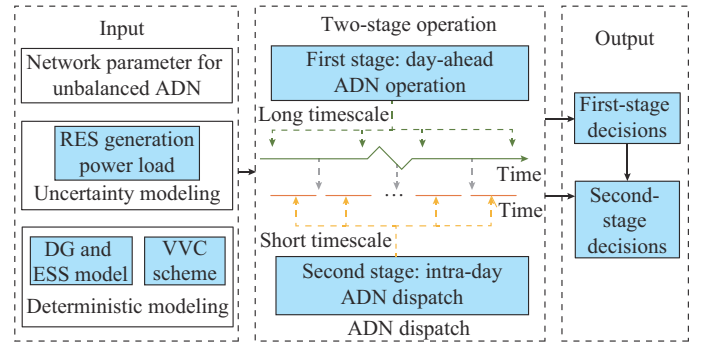


Fig. 4. Two-stage structure for unbalanced ADN operation.

The day-ahead ADN operation covers a longer timescale, with the given information of input prediction and operation parameters. In this paper, the day-ahead decisions include ESS charging/discharging power, on/off status of DEs, tap position of OLTC, and position levels of CB.

The intra-day ADN dispatch is conducted in a much shorter operation timescale, normally no more than one hour. The intra-day decisions will be made after the realization of various uncertainties and the operational decisions from the day-ahead stage [11]. The decisions for intra-day operation include active/reactive power dispatch of DEs, power exchange with the main grid, reactive power of WT and PV, active/reactive power flow, root branch power flow, and three-phase power unbalance. These decisions would be hourly updated and then executed to compensate for the day-ahead ADN operation.

The classification of the two stages depends on the different roles each unit plays and its response speed. ESS schedule is decided in the first stage since it mainly contributes to peakshaving and flexibility improvement over long-time periods. Besides, charging or discharging frequently would incur a higher degradation cost (19) and shorten its lifespan. The

CB status and OLTC status are also scheduled in the first stage, as they cannot respond fast and the frequent movements could reduce their lifetime dramatically [10].

D. Two-stage SP Method

To deal with diverse uncertainties, massive scenarios can be generated considering correlations among all the uncertainty sources in Section III-A. However, too many scenarios would lead to an excessively high computational burden. To improve the solution efficiency, the scenario reduction method and simultaneously backward reduction (SBR) technique can be utilized to select a rather small but representative scenario set [10]. Detailed information on the SBR method can be found in [29]. Afterward, the overall two-stage SP problem can be formulated as:

$$\begin{cases} \text{obj} = \min_{m, y_1, y_2, \dots, y_s} \left(D(m) + \sum_{s=1}^{N_s} \rho_s L(y_s) \right) \\ \text{s.t. } m \in CD_m | z \\ y_s \in CL(m, \Psi_s) \\ \forall s \in N_s \end{cases} \quad (51)$$

In (51), $D(m)$ is the objective of the day-ahead stage related to (17), (19), (22), and (23), and m denotes all the corresponding decisions discussed in Section III-B; s is the index of the representative scenarios; CD_m is the constraint set, including (28)-(32) and (36)-(39), related to the decision m ; N_s is the number of total scenarios; ρ_s is the probability of scenario; $L(y_s)$ is the object of intra-day ADN dispatch after revealing the uncertainties, consisting of (16), (18), (20), and (21), in which y_s is the intra-day decision variable; and $CL(m, \Psi_s)$ is the constraint set, involving (7)-(9), (24)-(27), and (33)-(35), corresponding to the decision y_s . It is noteworthy that the proposed two-stage SP method has some limitations, including the fixed stochastic variations and limited scenario numbers, which can be regarded as the future research direction of the SP method.

V. CASE STUDY

A. Test System

The proposed method is validated via an IEEE 34-bus distribution system, whose topology is shown in Fig. 5 and the detail of the system data can be found in [30] and [31]. The detailed parameter of unbalanced load for each phase in the IEEE 34-bus distribution system can be referred to [31], [32].

The bus voltage limit is set to be [0.95 p.u., 1.05 p.u.]; the substation voltage V_{sub} is 1 p.u.; the tap range of substation is set to be 5% with 20 tap positions, so $Tap_{min} = -10$ and $Tap_{max} = 10$. There are five CBs installed at all three phases of the buses 812, 850, 824, 862, and 834, with the same capacity of 300 kvar for each unit [10]. DE and ESS are installed at the buses 808, 832, 840, and 860 and the buses 808, 840, 848, and 860 [3]. Their locations are presented in Fig. 5, indicating they are installed in three phases, while RES is installed in either single or double phases shown by the different colors of the circle in Fig. 5. The capacity of

each DE is 150 kW with a ramping rate of 15 kW/min [33], [34]. The capacity of each ESS module is 120 kW/240 kWh, whose charging/discharging rate and decay rate are set to be 95% and 99.9%, respectively [3], [34]. The unit degradation cost for each charging and discharging events of ESS is 0.03 \$/kWh [25]. Furthermore, the maximum allowable power unbalances P_{unb}^{max} is set to be 0.18 p.u. and the overall system unbalance limit Unb_{total}^{max} is 1.07 p.u. [3].

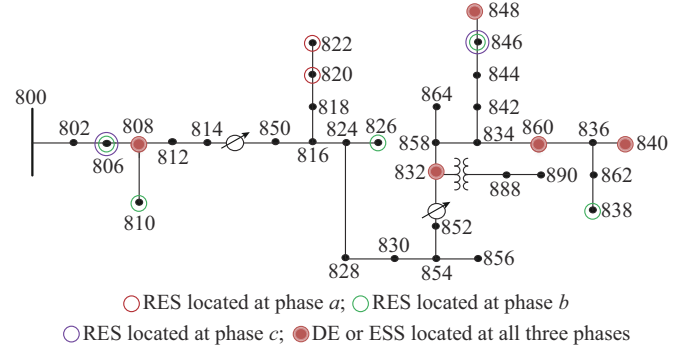


Fig. 5. Topology of IEEE 34-bus distribution system.

The energy tariffs [11] and other cost parameters are provided in Table I [35], [36]. The ESS degradation parameters are $L_{ESS,R}^{p,i} = 2190$, $\chi^0 = 4580$, $\chi^1 = 1.98$, and $DoD_R^{p,i} = 0.8$ [15]. The stochastic variations of RES generations and power loads are set to be 30% and 10%, respectively [11], [37]. The predictions of RES generation and power demands are given in Fig. 6. The day-ahead operation horizon is 24 hours with 1 hour granularity, and the timescale of intra-day dispatch is 1 hour.

TABLE I
ENERGY TARIFFS AND OTHER COST PARAMETER

Parameter	Price (\$/kW)
DE maintenance cost	0.0288
RES maintenance cost	0.0093
RES curtailment cost	0.0050
Power transaction	0.0768 (during 00:00-06:00, 23:00-24:00)
	0.1276 (during 06:00-08:00, 11:00-17:00)
	0.1696 (during 08:00-11:00, 17:00-22:00)

All the case studies are conducted on an Intel^(R) Core^(TM) i5-10500U CPU @ 3.10 GHz PC with 16 GB RAM and solved by Gurobi through Pyomo (version 6.0.1) package on Python.

B. Day-ahead Operation Results

Based on the historical data of RES generation and power loads, 1000 scenarios are generated by applying copula theory and reduced to 10 representative scenarios by the SBR technique [29]. To show the correlation among WT, PV, and demand, a comparison of 300 samples and 500 samples via copula theory is presented in Fig. 7. All the samples are generated when PV generation is almost at the peak of the day (12:00 a.m.). It is obvious from Fig. 7 that, at a single time point, whether we generate 300, 500, or 1000 samples, there

is an area in the scatter plot where all the samples cluster, showing the strenuous correlations among WT, PV, and loads.

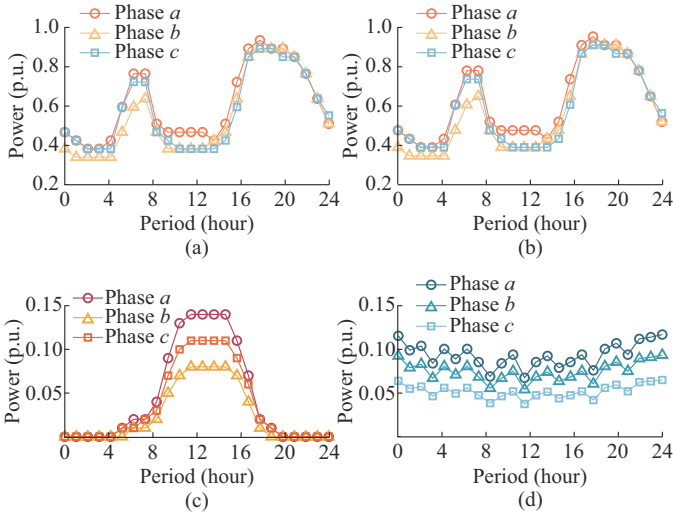


Fig. 6. Predictions of RES generation and power demands. (a) Active power demands. (b) Reactive power demands. (c) PV output. (d) WT output.

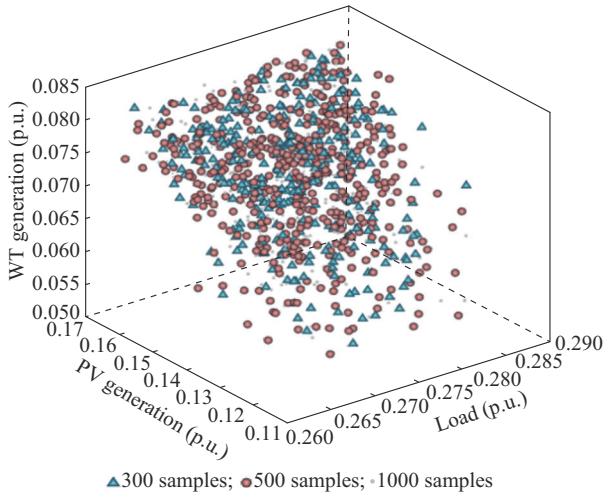


Fig. 7. Comparison of 300 samples and 500 samples via copula theory.

The OLTC tap positions and the voltage profile of the reference bus are presented in Fig. 8. The results indicate that the tap position is positive at most of the time, implying that the primary bus voltage is a bit higher than the nominal voltage level. This is reasonable as the system has high demand but not much RES injection. If the primary bus voltage is higher, the system can avoid the voltage falling below 0.95 p.u., while meeting a great amount of demand.

To demonstrate the impact of an unbalanced ADN on day-ahead operation decisions, the power output results of ESS are shown in Fig. 9, where the charging/discharging event of ESS on each phase happens during the same dispatch period to attain cost-saving goals and meet the demand. However, since most RESs are installed in phase *a* and phase *c*, the magnitude of power during each charging/discharging event of ESS is greater than the power in phase *b*. The ESS charging/discharging on phases *a* and *c* can also limit the voltage

rise induced by RES injection and mitigate the power unbalance.

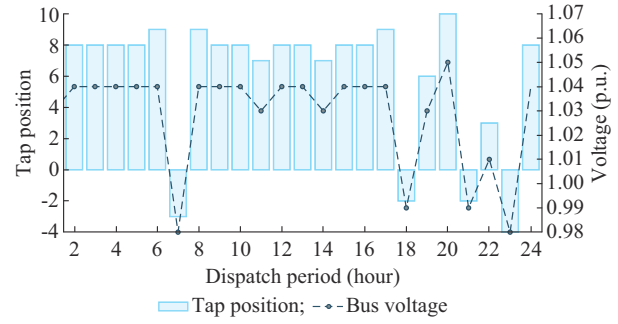


Fig. 8. OLTC tap positions and voltage profile of reference bus.

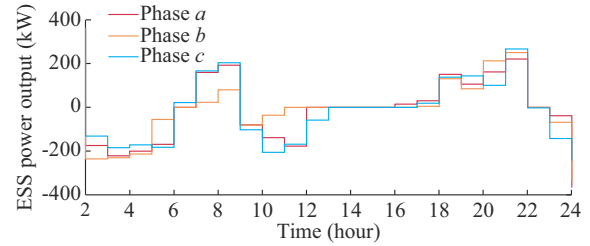


Fig. 9. Power output results of ESS.

The solution time of the proposed day-ahead operation is 1656.41 s, which indicates that the proposed method is compatible with real-world applications and efficient enough for the day-ahead operation.

C. Intra-day ADN Dispatch Results

The intra-day ADN dispatch is conducted on hourly bases with the realization of RES and load uncertainties. The simulation results are demonstrated in Figs. 10 to 13.

Figure 10 indicates that all the generation units are scheduled optimally based on the objective while meeting the operational constraints. Since RES generation cannot fully meet the demand based on the input prediction, DE contributes to supplying the rest of the demand. For the periods from hour 17 to hour 22, DE reaches its maximum output so that the system is allocated to purchase the power from the main grid. The ESS could attain the goals of peakshaving and operation cost saving of the power load. ESS charges during the periods from hour 2 to hour 5 when both the demand and power transaction price are the lowest of the day. ESS discharges during high power transaction periods from hour 17 to hour 21 to meet the peak demand. Additionally, with the consideration of the battery degradation effect in (19), charging/discharging events of ESS cannot happen frequently over the entire dispatch horizon since numerous ESS operations would induce high degradation costs.

The reactive power balance is presented in Fig. 11. Compared with phase *a* and phase *c*, phase *b* has the lowest RES installation, hence, the reactive power balance is supplied by CB most of the time, even during the peak time of PV generation. For phase *a* and phase *c*, the reactive power from the RES inverters is the priority of reactive power balance. The rest of the reactive loads is mainly satisfied by CB, while

the reactive power support from the main grid is almost zero. This is because the local reactive power supply contributes to loss reduction.

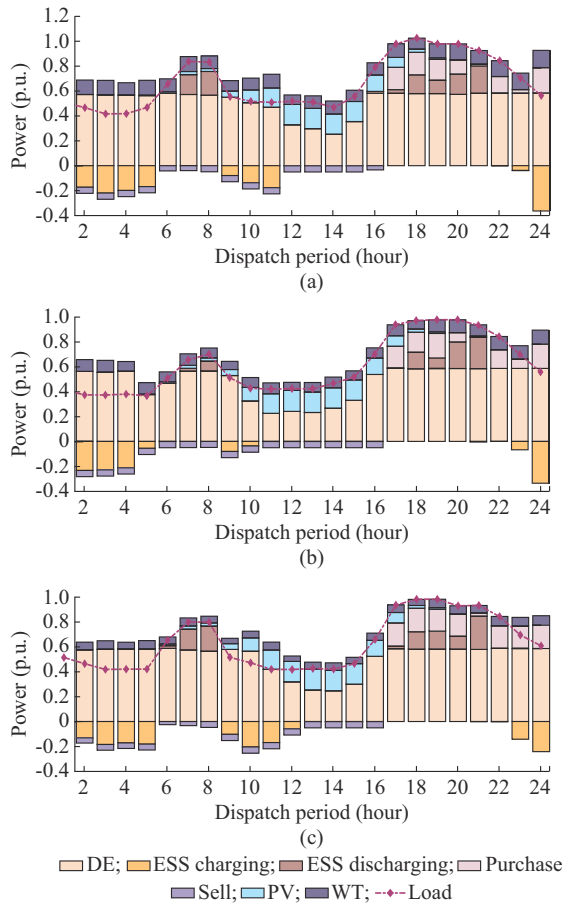


Fig. 10. Intra-day active power dispatch results for three phases. (a) Phase a. (b) Phase b. (c) Phase c.

Moreover, the hourly root branch three-phase active power unbalance are depicted in Fig. 12, which illustrate that critical power unbalance occurs at nighttime during ESS charging. It is worth noting that the power unbalances of all the scenarios are within the predefined limits. To further demonstrate the impact of an unbalanced ADN on intra-day ADN dispatch results, the DE power outputs are shown in Fig. 13. It shows that DE generation in phase b is apparently lower than in the other two phases, as the demand in phase b is lower than in phase a and phase c.

The intra-day ADN dispatch results verify the effectiveness of the proposed method of coordination of all the DER units and reactive power devices to attain both optimal active and reactive power managements. The final cost of intra-day ADN dispatch over 24 hours is \$8978.32 and the solving time for the intra-day operation is 6.24 s for each hour. This solution performance also validates that the proposed method is compatible with the intra-day operation.

D. Comparison with Other Methods

To illustrate the validness and effectiveness of the proposed method, other unbalanced distribution system operation benchmarks are compared.

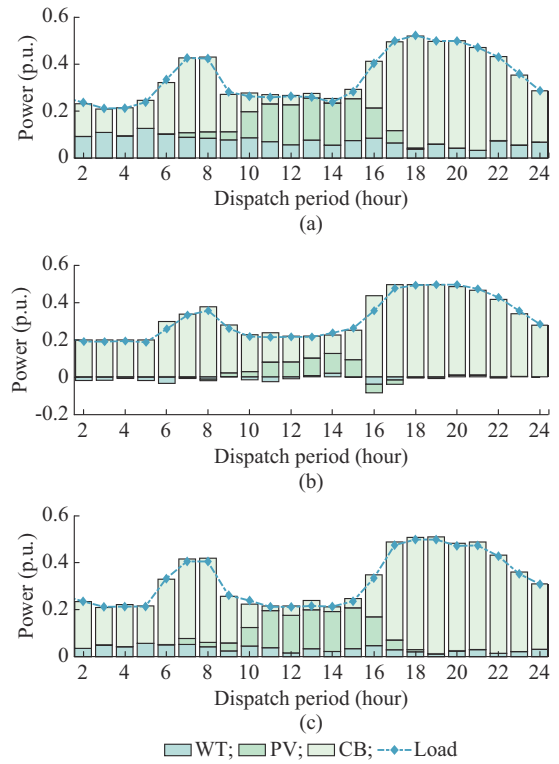


Fig. 11. Intra-day reactive power dispatch results for three phases. (a) Phase a. (b) Phase b. (c) Phase c.

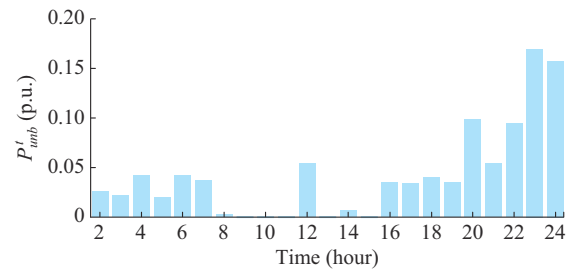


Fig. 12. Hourly root branch three-phase active power unbalance.

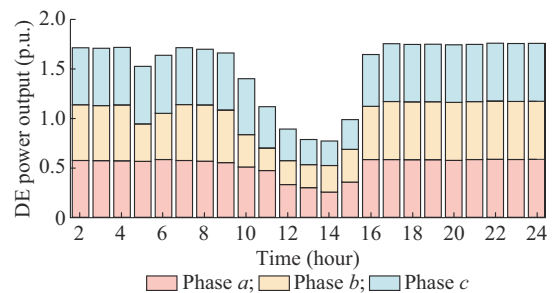


Fig. 13. DE power outputs.

Method A (MA): this is the deterministic operation method and the forecast of the RES generation and load are regarded as accurate [2], [38].

Method B (MB): the centralized VVC scheme is not involved. This means the coordination between active and reactive power dispatch does not exist and all the reactive power is satisfied by only renewable inverters and the main grid [3], [18], [35].

Method C (MC): the ESS degradation is not considered where the ESS capacity assumes to be constant during each charging/discharging event [18], [35].

The optimization results of these benchmarks are demonstrated in Table II. Besides, one of the comparing criteria called the hourly unbalance rate Unb^{avg} , which is the average of three-phase unbalance P_{unb}^t , is defined in (52).

$$Unb^{avg} = \frac{1}{N_t} \sum_{t \in N_t} P_{unb}^t \quad (52)$$

TABLE II
COMPARISON OF SIMULATION RESULTS

Method	First stage		Second stage			
	Operation cost (\$)	Solution time (s)	Operation cost (\$)	Power loss cost (\$)	Hourly unbalance rate (p.u.)	Solution time (s)
MA	8395	23	8778	244	0.023	6.37
MB	8835	812	9128	458	0.045	6.72
MC	8534	424	8856	243	0.039	6.08
Proposed	8633	1656	8978	244	0.042	6.24

From the comparison of simulation results in Table II, it can be inferred that:

1) For MA, the system operation cost and power loss cost are lower compared with all methods with the least solution time. This is rational as only one scenario is considered with a smaller problem dimension. However, for this method, it is not practical because in reality, the accuracy of uncertainty predictions cannot be guaranteed completely.

2) For MB, without the modeling of the VVC scheme, the reactive power balance is only supported by the main utility. The transmission of a great amount of power to a single bus will scarify higher power loss costs. It can be observed that the power loss cost in MB is twice as high as the proposed method. Hence, to reduce the power losses and build up a cost-effective model, the coordination of active and reactive power is necessary to be considered in the ADN operation.

3) For MC, the constraints in terms of ESS degradation are ignored, and the operation cost is lower than the proposed method with a better computational performance since the linearization of ESS degradation involves many binary variables. However, the neglect of ESS degradation leads to imprecise and idealistic results.

4) Compared with MA to MC, the proposed method has lower power loss and reasonable operation costs. Unb^{avg} of the proposed method is similar to those of MB and MC. Because the three-phase imbalance is mainly about active power dispatch and if the reactive power optimization is ignored in MB, it would not influence the active power scheduling and the three-phase unbalanced power. From Table II, the obtained results for the second stage are slightly higher than the first-stage operation cost results. Those differences are brought by the impact of the individual scenario in the second-stage simulation. The results from the first stage are the expected value of all the various covered scenarios, while the second stage is significantly affected by the revealed uncertainty.

E. Sensitivity Analysis for Number of Different Scenarios

To further indicate the effectiveness of the proposed method, the sensitivity analysis is conducted based on different numbers of scenarios. As the proposed method is solved with 10 scenarios reduced from 1000 scenarios, for the comparison, 5, 15, and 20 scenarios are utilized. The comparison of different numbers of scenarios is listed in Table III, where S5 to S20 means we use 5 to 20 scenarios for simulation.

TABLE III
COMPARISON OF DIFFERENT NUMBERS OF SCENARIOS

Item	Power loss cost (\$)	Hourly unbalance (p.u.)	Solution time (s)
S5	327.76	0.0443	598
S10	244.86	0.0421	1656
S15	246.94	0.0417	19519
S20	248.82	0.0435	65499

The results show that there is a significant difference in system operation cost and power loss cost between S5 and S10. This is because for fewer scenario cases, each scenario has a critical impact on the simulation results and a single extreme case will greatly affect the system cost. With the increasing number of scenarios, the results are similar but a longer solution time is taken. From the sensitivity analysis results, it can be observed that 10 scenarios can be enough to balance the solution accuracy and solution time.

F. Sensitivity Analysis for Three-phase Unbalanced Limits

To illustrate the impact of changing the power unbalance limits on the system operation, we have selected four extra cases (cases 1-4) whose three-phase power unbalances are 20% and 10% lower than the proposed method; and 20% and 10% higher than the proposed method, for which $P_{unb}^{max} = 0.18$ p.u. and $Unb_{total}^{max} = 1.07$ p.u.. Taking case 1 as an example, P_{unb}^{max} and Unb_{total}^{max} are set to be 20%, which are lower than the proposed method, and $P_{unb,1}^{max} = 0.144$ p.u., $Unb_{total,1}^{max} = 0.856$ p.u.. The results of this sensitivity analysis are presented in Fig. 14, where the proposed method is also involved to make the best comparison. The indicator of hourly average unbalance is in (52).

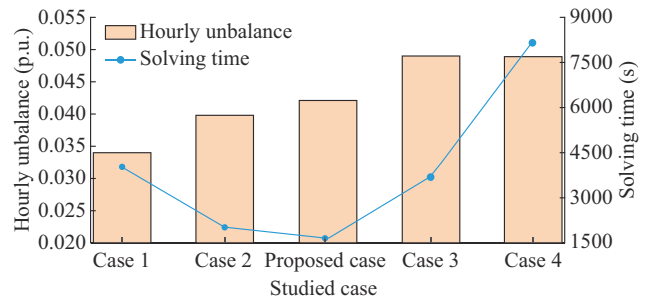


Fig. 14. Results of sensitivity analysis for three-phase power unbalance limits.

From Fig. 14, with the decrease of P_{unb}^{max} , the hourly unbalance rate is reduced as well to meet the system constraints. However, the solution time gradually increases as the system limits become narrower. The dramatic rise of the solving

time with the increase of P_{unb}^{\max} is witnessed by cases 3 and 4. Considering that the limits of the root branch three-phase unbalance are broadened, it would enlarge the range of other decision variables and bring a significant effect on the computing performance. Despite the large changes in the solving time, relatively small differences are found in terms of Unb^{avg} between cases 3 and 4. Even though (the limits of widened root branch three-phase unbalance) are considered, the system should still meet the voltage and power flow limits to guarantee the safe operation of the ADN. Based on the analysis above, the proposed method marginally outperforms the other methods by the minimum solving time and acceptable hourly unbalance.

VI. CONCLUSION

This paper proposes an optimal coordinated operation method for the unbalanced ADN. The active and reactive power can be jointly optimized by utilizing the VVC scheme to regulate the voltage and reduce the power losses. The ESS degradation model is also considered to characterize the aging impact of each charging/discharging event. Copula theory is applied for handling uncertainty by recognition of correlations of all the uncertainty sources. Finally, numerical case studies are conducted to illustrate the following aspects.

1) The linearized three-phase branch flow model can schedule DER output differently among three phases and derive a more precise and realistic operation cost. The ESS aging cost also verifies that the degradation process has a neglectable impact on system cost.

2) The proposed method enables the joint optimization of the active and reactive power effectively in the unbalanced ADN. Besides, the power losses can be effectively reduced.

3) The copula-based two-stage SP method could correctly reveal the correlation between dependent uncertain variables, which effectively addresses the diverse uncertainties.

REFERENCES

- [1] M. J. Ghadi, S. Ghavidel, A. Rajabi *et al.*, "A review on economic and technical operation of active distribution systems," *Renewable and Sustainable Energy Review*, vol. 104, pp. 38-53, Jan. 2019.
- [2] Z. Wang, J. Wang, and C. Chen, "A three-phase microgrid restoration model considering unbalanced operation of distributed generation," *IEEE Transactions on Smart Grid*, vol. 9, no. 4, pp. 3594-3604, Jul. 2018.
- [3] B. Wang, C. Zhang, Z. Y. Dong *et al.*, "Improving hosting capacity of unbalanced distribution networks via robust allocation of battery energy storage systems," *IEEE Transactions on Power Systems*, vol. 36, no. 3, pp. 2174-2185, May 2021.
- [4] B. Zhou, J. Zou, C. Y. Chung *et al.*, "Multi-microgrid energy management systems: architecture, communication, and scheduling strategies," *Journal of Modern Power Systems and Clean Energy*, vol. 9, no. 3, pp. 463-476, May 2021.
- [5] M. Farivar and S. H. Low, "Branch flow model: relaxations and convexification: Part I," *IEEE Transactions on Power Systems*, vol. 28, no. 3, pp. 2554-2564, Aug. 2013.
- [6] J. Teng, "A direct approach for distribution system load flow solutions," *IEEE Transactions on Power Delivery*, vol. 18, no. 3, pp. 882-887, Jul. 2003.
- [7] L. Gan and S. H. Low, "Convex relaxations and linear approximation for optimal power flow in multiphase radial networks," in *Proceedings of 2014 Power System Computation Conference*, Wroclaw, Poland, Aug. 2014, pp. 1-9.
- [8] C. Chen, F. Wang, B. Zhou *et al.*, "An interval optimization based day-ahead scheduling scheme for renewable energy management in smart distribution systems," *Energy Conversion and Management*, vol. 106, pp. 584-596, Dec. 2015.
- [9] R. H. A. Zubo, G. Mokryani, H. S. Rajamani *et al.*, "Operation and planning of distribution networks with integration of renewable distributed generators considering uncertainties: a review," *Renewable and Sustainable Energy Review*, vol. 72, pp. 1177-1198, Oct. 2017.
- [10] Y. Xu, Z. Y. Dong, R. Zhang *et al.*, "Multi-timescale coordinated voltage/var control of high renewable-penetrated distribution systems," *IEEE Transactions on Power Systems*, vol. 32, no. 6, pp. 4398-4408, Nov. 2017.
- [11] Z. Li, L. Wu, and Y. Xu, "Risk-averse coordinated operation of a multi-energy microgrid considering voltage/var control and thermal flow: an adaptive stochastic approach," *IEEE Transactions on Smart Grid*, vol. 12, no. 5, pp. 3914-3927, Sept. 2021.
- [12] K. Mahmoud, M. M. Hussein, M. Abdel-Nasser *et al.*, "Optimal voltage control in distribution systems with intermittent PV using multi-objective Grey-Wolf-Lévy optimizer," *IEEE Systems Journal*, vol. 14, no. 1, pp. 760-770, Mar. 2020.
- [13] R. Zafar, J. Ravishankar, J. E. Fletcher *et al.*, "Multi-timescale model predictive control of battery energy storage system using conic relaxation in smart distribution grids," *IEEE Transactions on Power Systems*, vol. 33, no. 6, pp. 7152-7161, Nov. 2018.
- [14] D. Jin, H. D. Chiang, and P. Li, "Two-timescale multi-objective coordinated volt/var optimization for active distribution networks," *IEEE Transactions on Power Systems*, vol. 34, no. 6, pp. 4418-4428, Nov. 2019.
- [15] Y. Zhang, Y. Xu, H. Yang *et al.*, "Optimal whole-life-cycle planning of battery energy storage for multi-functional services in power systems," *IEEE Transactions on Sustainable Energy*, vol. 11, no. 4, pp. 2077-2086, Oct. 2020.
- [16] C. Ju, P. Wang, L. Goel *et al.*, "A two-layer energy management system for microgrids with hybrid energy storage considering degradation costs," *IEEE Transactions on Smart Grid*, vol. 9, no. 6, pp. 6047-6057, Nov. 2018.
- [17] B. Zhou, X. Liu, Y. Cao *et al.*, "Optimal scheduling of virtual power plant with battery degradation cost," *IET Generation, Transmission & Distribution*, vol. 10, no. 3, pp. 712-725, Jun. 2016.
- [18] Y. Liu, L. Guo, and C. Wang, "A robust operation-based scheduling optimization for smart distribution networks with multi-microgrids," *Applied Energy*, vol. 228, pp. 130-140, Mar. 2018.
- [19] S. M. Mohseni-Bonab, I. Kamwa, A. Moeini *et al.*, "Voltage security stochastic programming model for day-ahead BESS schedule in co-optimization of T&D systems," *IEEE Transactions on Sustainable Energy*, vol. 11, no. 1, pp. 391-404, Jan. 2020.
- [20] X. Wang, Z. Hu, M. Zhang *et al.*, "Two-stage stochastic optimization for unit commitment considering wind power based on scenario analysis," in *Proceedings of 2016 China International Conference on Electricity Distribution (CICED)*, Xi'an, China, Aug. 2016, pp. 1-5.
- [21] D. Yu and N. Ghadimi, "Reliability constraint stochastic UC by considering the correlation of random variables with Copula theory," *IET Renewable Power Generation*, vol. 13, no. 14, pp. 2587-2593, Jul. 2019.
- [22] Y. Chi, Y. Xu, and T. Ding, "Coordinated var planning for voltage stability enhancement of a wind-energy power system considering multiple resilience indices," *IEEE Transactions on Sustainable Energy*, vol. 11, no. 4, pp. 2367-2379, Oct. 2020.
- [23] B. Chen, C. Chen, J. Wang *et al.*, "Sequential service restoration for unbalanced distribution systems and microgrids," *IEEE Transactions on Power Systems*, vol. 33, no. 2, pp. 1507-1520, Mar. 2018.
- [24] R. R. Jha, A. Dubey, C.-C. Liu *et al.*, "Bi-level volt-var optimization to coordinate smart inverters with voltage control devices," *IEEE Transactions on Power Systems*, vol. 34, no. 3, pp. 1801-1813, May 2019.
- [25] Y. Zhang and M.-Y. Chow, "Microgrid cooperative distributed energy scheduling (CoDES) considering battery degradation cost," in *Proceedings of 2016 IEEE 25th International Symposium on Industrial Electronics (ISIE)*, Santa Clara, USA, Nov. 2016, pp. 720-725.
- [26] Y. Chi, Y. Xu, and R. Zhang, "Candidate bus selection for dynamic var planning towards voltage stability enhancement considering copula-based correlation of wind and load uncertainties," *IET Generation, Transmission & Distribution*, vol. 15, no. 4, pp. 780-791, Oct. 2020.
- [27] P. Li, X. Guan, J. Wu *et al.*, "Modeling dynamic spatial correlations of geographically distributed wind farms and constructing ellipsoidal uncertainty sets for optimization-based generation scheduling," *IEEE Transactions on Sustainable Energy*, vol. 6, no. 4, pp. 1594-1605, Oct. 2015.
- [28] A. J. Patton, "A review of copula models for economic time series,"

- Journal of Multivariate Analysis*, vol. 110, pp. 4-18, Sept. 2012.
- [29] Y. Chen, X. Feng, Z. Li *et al.*, "Multi-stage coordinated operation of a multi-energy microgrid with residential demand response under diverse uncertainties," *Energy Conversion and Economics*, vol. 1, no. 1, pp. 20-33, Oct. 2020.
- [30] W. H. Kersting, "Radial distribution test feeders," *IEEE Transactions on Power Systems*, vol. 6, no. 3, pp. 975-985, Aug. 1991.
- [31] IEEE. (2022, Jan.). IEEE 34 node test feeder. [Online]. Available: <https://cmte.ieee.org/pes-testfeeders/resources/>
- [32] A. Ulinuha, M. A. S. Masoum, and S. M. Islam, "Unbalance power flow calculation for a radial distribution system using forward-backward propagation algorithm," in *Proceedings of 2007 Australasian Universities Power Engineering Conference*, Perth, Australia, Dec. 2007, pp. 1-6.
- [33] S. Chen, H. B. Gooi, and M. Wang, "Sizing of energy storage for microgrids," *IEEE Transactions on Smart Grid*, vol. 3, no. 1, pp. 142-151, Mar. 2012.
- [34] Z. Li and Y. Xu, "Optimal coordinated energy dispatch of a multi-energy microgrid in grid-connected and islanded modes," *Applied Energy*, vol. 210, pp. 974-986, May 2018.
- [35] Z. Li and Y. Xu, "Temporally-coordinated optimal operation of a multi-energy microgrid under diverse uncertainties," *Applied Energy*, vol. 240, pp. 719-729, Apr. 2019.
- [36] Z. Li, Y. Xu, X. Feng *et al.*, "Optimal stochastic deployment of heterogeneous energy storage in a residential multienergy microgrid with demand-side management," *IEEE Transactions on Industrial Informatics*, vol. 17, no. 2, pp. 991-1004, Feb. 2021.
- [37] C. Zhang, Z. Y. Dong, and Y. Xu, "Two-stage robust operation for islanded multi-energy micro-grids," in *Proceedings of The 11th IET International Conference on Advances in Power System Control, Operation and Management (APSCOM 2018)*, Hong Kong, China, Nov. 2018, pp. 1-10.
- [38] A. Das, Z. Ni, T. M. Hansen *et al.*, "Energy storage system operation: case studies in deterministic and stochastic environments," in *Proceedings of 2016 IEEE PES Innovative Smart Grid Technologies Conference (ISGT)*, Niagara Falls, Canada, Sept. 2016, pp. 1-5.
- Ruoxuan Leng** received the B.E. degree in electrical and electronic engineering from both University of Edinburgh, Scotland, UK, and North China Electric Power University, Beijing, China, in 2020. She is currently a Ph.D. Student in School of Electrical and Electronic Engineering, Nanyang Technological University, Singapore. Her research interests include optimal operation and planning of distributed energy resources.
- Zhengmao Li** received the B.E. degree in information engineering and the M.E. degree in electrical engineering from Shandong University, Jinan, China, in 2013 and 2016, respectively, and the Ph.D. degree in electrical engineering from the School of Electrical and Electronic Engineering, Nanyang Technological University, Singapore, in 2020. During 2019-2021, he was a Research Fellow with the Stevens Institute of Technology, Hoboken, USA, and he is currently a Research Fellow with Nanyang Technological University under the NTU-ETH Project. His research interests include renewable energy integration, microgrid, and multi-energy system, and optimization techniques such as approximate dynamic programming, robust optimization, and stochastic optimization.
- Yan Xu** received the B.E. and M.E degrees from South China University of Technology, Guangzhou, China, in 2008 and 2011, respectively, and the Ph.D. degree from The University of Newcastle, Newcastle, Australia, in 2013. He conducted postdoctoral research with the University of Sydney Postdoctoral Fellowship, Sydney, Australia, and then joined Nanyang Technological University (NTU) with The Nanyang Assistant Professorship, Singapore. He is now an Associate Professor at School of Electrical and Electronic Engineering and a Cluster Director at Energy Research Institute @ NTU (ERI@N), Singapore. He is an Editor for IEEE Transactions (TSG and TPWRS), IET Journals (GTD and ECE), and Journal of Modern Power Systems and Clean Energy and CSEE JPES. He is also serving as the Chairman for IEEE Power & Energy Society Singapore Chapter. His research interests include power system stability and control, microgrid, and data analytics for smart grid applications.